Available online at www.sciencedirect.com
ScienceDirect
Bioorganic & Medicinal Chemistry Letters 18 (2008) 732–737
Bioorganic & Medicinal Chemistry Letters

Thiol-based angiotensin-converting enzyme 2 inhibitors: P^1 modifications for the exploration of the S^1 subsite

David N. Deaton,[a,*] Enoch N. Gao,[b] Kevin P. Graham,[b] Jeffrey W. Gross,[b] Aaron B. Miller[c] and John M. Strelow[b]

[a]*Department of Medicinal Chemistry, GlaxoSmithKline, Research Triangle Park, NC 27709, USA*
[b]*Molecular Discovery Research, Screening & Compound Profiling, GlaxoSmithKline, Upper Providence, PA 19426, USA*
[c]*Molecular Discovery Research, Computational and Structural Chemistry, GlaxoSmithKline, Research Triangle Park, NC 27709, USA*

Received 13 September 2007; revised 12 November 2007; accepted 14 November 2007
Available online 19 November 2007

Abstract—Screening of a metalloprotease library led to the identification of a thiol-based dual ACE/NEP inhibitor as a potent ACE2 inhibitor. Modifications of the P^1 benzyl moiety led to improvements in ACE2 potency as well as to increased selectivity versus ACE and NEP.

Angiotensin-converting enzyme 2 (ACE2) is a recently identified clan MA, family M2 monocarboxypeptidase with highest homology to the dicarboxypeptidase angiotensin-converting enzyme (ACE, EC 3.4.15.1).[1,2] This membrane-associated and secreted metalloprotease is expressed in heart, kidney, testes, intestine, and lung, and has been implicated in cardiovascular disease, kidney disease, obesity, and lung disease.[3–5]

ACE2 processes angiotensin I and the AT_1 and AT_2 receptor agonist angiotensin II to produce angiotensin (1–9) and the *mas* receptor agonist angiotensin (1–7), respectively, but its exact role in the renin-angiotensin system (RAS) needs to be clarified. One group has reported that C57BL/6 ACE2 (−/−) mice exhibit a severe reduction in cardiac contractility, which is rescued in the ACE (−/−)/ACE2 (−/−) double knockout.[6] In contrast, another group has disclosed that ACE2 (−/−) mice of 129/SvEv, C57BL/6, and mixed background do not exhibit cardiac contractility defects, but have increased susceptibility to angiotensin II-induced hypertension.[7] While, a third group has revealed that male ACE (−/Y) mice are more susceptible to heart failure and death after transverse aortic constriction than their normal littermates.[8] Supporting a role for ACE2 in cardiac function, transgenic mice overexpressing ACE2 in the heart have lower mean arterial pressure with rare focal myocyte vacuolization, myofibril splaying, and nuclear enlargement. Many of these mice develop terminal ventricular fibrillation with lethal arrhythmias.[9]

Furthermore, male ACE2 (−/Y) mice, but not female ACE2 (−/−) mice, also accumulate fibrillar collagen in the renal glomerular mesangium, leading to development of glomerulosclerosis of the kidneys.[10] In addition, ACE2 (−/−) mice exhibit lower body weights than wild type mice with reduced fat mass.[11] Moreover, ACE2 is also utilized by the severe acute respiratory syndrome (SARS) coronavirus as the receptor for infection.[12] ACE2 (−/−) mice are resistant to SARS corona virus infection.[13] Finally, ACE2 (−/−) mice have enhanced vascular permeability, increased lung edema, and worsened lung function in several murine acute respiratory distress syndrome (ARDS) models.[14] With the many potential functions of ACE2, small molecule inhibitors of this enzyme could be utilized to help further define the physiological roles of this protease.

ACE2 belongs to the zinc metalloprotease family and it has been reported that classical ACE inhibitors such as captopril and lisinopril do not attenuate ACE2 enzyme activity. As part of a strategy to discover lead molecules for an ACE2 inhibitor program, a directed screen of ACE2 versus a set of metalloprotease inhibitors from

Keywords: Angiotensin-converting enzyme 2; Metalloproteases; Protease inhibitors; Thiols.
* Corresponding author. Tel.: +1 919 483 6270; fax: +1 919 315 0430; e-mail: david.n.deaton@gsk.com

0960-894X/$ - see front matter © 2007 Elsevier Ltd. All rights reserved.
doi:10.1016/j.bmcl.2007.11.048

the GlaxoSmithKline compound collection was performed. Surprisingly, although confirming that classical ACE inhibitors like captopril were inactive in the screen, the thiol acid **1a** was identified as a potent ACE2 inhibitor ($K_{i\ App}$ = 86 nM).[15] This biphenyl analog **1a** is a known dual ACE and M13 metalloprotease neutral endopeptidase (neprilysin, NEP, EC 3.4.24.11) inhibitor (ACE $K_{i\ App}$ = 30 nM, NEP $K_{i\ App}$ = 1.1 nM).[16] It also inhibits the M14 metalloprotease carboxypeptidase A1 (CpA, EC 3.4.17.1, $K_{i\ App}$ = 1,200 nM). Speculating that the thiol functioned as a binding group for the active site zinc and that the carboxylic acid served as a recognition element for the enzyme's monocarboxypeptidase activity, the benzyl and methylene *p*-biphenyl moieties were surmised to be the P^1 and $P^{1'}$ substituents. With this premise, the structure activity relationships of the P^1 position of the lead inhibitor were explored with the goal of improving potency and reducing ACE and NEP inhibitory activity.

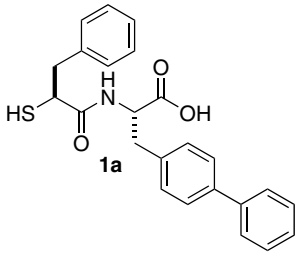

1a

The thiol analogs **1a**–**1s** were prepared as depicted in Scheme 1. The acids **3a**–**3s** were activated in situ via the carbodiimide, converted into the activated esters with the aza-hydroxybenzotriazole, and then coupled to the amine hydrochloride **4** to produce the fully protected amides. Subsequent hydrolysis of the methyl ester, as well as the thioacetate, with lithium hydroxide afforded the thiol acids **1a**–**1s**.[17]

The thiol acids **3a**–**3s** were produced by three different routes. Acids **3c** and **3e** were prepared by reaction of the commercially available thiols **2c** and **2e** (X=S) with acetyl chloride. In contrast, the acids **3k**, **3m**, and **3n** were produced from the alcohols **2k**, **2m**, and **2n** (X=O) via the Mitsunobu reaction with thioacetic acid.[18] Alternatively, the acids **3a**–**3b**, **3d**, **3f**–**3j**, **3l**, and **3o**–**3s** were synthesized from the commercially available

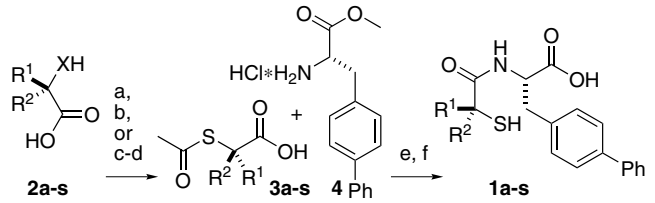

2a-s **3a-s** **4** **1a-s**

Scheme 1. Reagents and conditions: (a) **2c** and **2e**, X=S, AcCl, NEt_3, dioxane, 0 °C to rt, 15–37%; (b) **2k**, **2m**, and **2n**, X=O, AcSH, DIAD, PPh_3, THF, 0 °C to rt, 24–67%; (c) **2a**–**2b**, **2d**, **2f**–**2j**, **2l**, **2o**–**2s**, X=NH, HBr, $NaNO_2$, H_2O, 0 °C, 25–80%; (d) AcS^-K^+, DMF, 0 °C to rt, 11–72%; (e) EDC, HOAt, *i*-Pr_2NEt, CH_2Cl_2, 48–96%; (f) LiOH·H_2O, THF, H_2O, 30–94%.

amino acids **2a**–**2b**, **2d**, **2f**–**2j**, **2l**, and **2o**–**2s** (X=NH), by diazotization of the amines to afford the bromides, then subsequent displacement of the bromides, by potassium thioacetate, with stereochemical inversion. Some stereochemical erosion, presumably resulting from formation of the α-lactone before nucleophilic trapping, resulted during the Mitsunobu and diazotization reaction steps, but after coupling with the amine **4**, the minor diastereomer could be removed via chromatography.

The structure/activity relationships of P^1 analogs are depicted in Table 1. The (R) isomer **1b** derived from L-phenylalanine displays the P^1 benzyl substituent in the unnatural configuration. This orientation of the P^1 substituent was detrimental to the ACE2 inhibitory activity of diastereomer **1b** ($K_{i\ App}$ = 1400 nM) as well as that of ACE ($K_{i\ App}$ = 520 nM). This loss in inhibition is not surprising, since nature has evolved proteases to recognize the natural configuration of physiological peptide substrates. In contrast, NEP ($K_{i\ App}$ = 1.3 nM) accommodated the alternate configuration with no loss in potency.

Complete removal of the P^1 moiety caused a modest loss in inhibitory potency versus ACE2 (H, $K_{i\ App}$ = 320 nM). This decrease in potency could arise from reduced van der Waals interactions due to the lack of a P^1 substituent, the increased entropic cost for the inhibitor to bind to the protease given the inhibitor's increased rotational freedom, or a combination of these factors. In contrast to the D-isomer **1b**, the ACE activity ($K_{i\ App}$ = 16 nM) of the glycine-like analog **1c** was not affected by elimination of the P^1 element, while NEP potency ($K_{i\ App}$ = 13 nM) of **1c** decreased by over an order of magnitude.

The alanine-derived analog **1d** (Me, $K_{i\ App}$ = 6.9 nM) decreases rotational freedom and was an even more potent ACE2 inhibitor than the starting lead **1a**, while increasing selectivity versus both ACE ($K_{i\ App}$ = 21 nM) and NEP ($K_{i\ App}$ = 23 nM). In contrast, the geminal dimethyl analog **1e** (ACE2 $K_{i\ App}$ = 2300 nM) decreased inhibitory potency versus not only ACE2, but also ACE ($K_{i\ App}$ = 3,400 nM) and NEP ($K_{i\ App}$ = 730 nM). Similar to the methyl analog **1d**, the linear P^1 ethyl and *n*-butyl analogs **1f** (Et, $K_{i\ App}$ = 1.4 nM) and **1g** (*n*-Bu, $K_{i\ App}$ = 1.8 nM) were also potent ACE2 inhibitors, but these extensions in P^1 also increased activity versus ACE (**1f** $K_{i\ App}$ = 8.6 nM, **1g** $K_{i\ App}$ = 9.3 nM) and even more so versus NEP (**1f** $K_{i\ App}$ = 0.80 nM, **1g** $K_{i\ App}$ = 1.2 nM).

With the hope of improving the selectivity of these thiol-based inhibitors versus ACE and NEP, the effect of branching along the P^1 side chain of this inhibitor class was explored. Branching along the P^1 chain was well tolerated in the S^1 subsite of ACE2. The α-branched *iso*-propyl **1h** (*i*-Pr, $K_{i\ App}$ = 1.5 nM), (R)-*sec*-butyl **1i** ((R)-*s*-Bu, $K_{i\ App}$ = 1.5 nM), (S)-*sec*-butyl **1j** ((S)-*s*-Bu, $K_{i\ App}$ = 1.6 nM), cyclobutyl **1k** (Cyb, $K_{i\ App}$ = 2.4 nM), and cyclopentyl **1l** (Cyp, $K_{i\ App}$ = 1.8 nM) analogs and the β-branched *iso*-butyl **1o** (*i*-Bu, $K_{i\ App}$ = 1.4 nM)

Table 1. Inhibition of human ACE2, ACE, NEP, and CpA

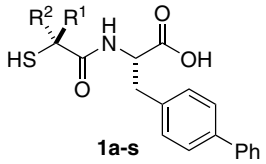

1a-s

#	R^1	R^2	ACE2 $K_{i\ App}$[a] (nM)	ACE $K_{i\ App}$[b] (nM)	NEP $K_{i\ App}$[c] (nM)	CpA $K_{i\ App}$[d] (nM)
1a	CH_2Ph	H	86	30	1.1	1200
1b	H	CH_2Ph	1400	520	1.3	310
1c	H	H	320	16	13	1700
1d	Me	H	6.9	21	23	14,000
1e	Me	Me	2300	3400	730	>50,000
1f	Et	H	1.4	8.6	0.80	9,300
1g	*n*-Bu	H	1.8	9.3	1.2	8900
1h	*i*-Pr	H	1.5	200	13	17,000
1i	(R)-s-Bu	H	1.5	490	27	11,000
1j	(S)-s-Bu	H	1.6	200	2.4	15,000
1k	Cyb	H	2.4	620	5.4	12,000
1l	Cyp	H	1.8	700	38	12,000
1m	Cyh	H	65	13,000	1300	12,000
1n	Ph	H	84	>10,000	410	>50,000
1o	*i*-Bu	H	1.4	3.2	0.28	11,000
1p	CH_2t-Bu	H	7.1	2,700	2.6	22,000
1q	CH_2Cyh	H	420	840	130	17,000
1r	$CH_2\beta$-Np	H	550	210	140	32,000
1s	$(CH_2)_2Ph$	H	860	93	2.6	5,000

[a] Inhibition of recombinant human ACE2 activity in a fluorescence assay using 0.4 nM ACE2, 30 μM MCA-Tyr-Val-Ala-Asp-Ala-Pro-Lys(DNP)-OH as substrate in 1 μM $Zn(OAc)_2$, 100 μM TCEP, 50 mM Hepes, 300 μM CHAPS, and 300 mM NaCl at pH = 7.5. The average percent coefficient of variance for the $K_{i\ App}$ values was 45%.

[b] Inhibition of recombinant human ACE activity in a fluorescence assay using 0.5 nM ACE, 10 μM MCA-Ala-Ser-Asp-Lys-Dap(DNP)-OH as substrate in 1 μM $Zn(OAc)_2$, 100 μM TCEP, 50 mM Hepes, 300 μM CHAPS, and 300 mM NaCl at pH = 7.5. The average percent coefficient of variance for the $K_{i\ App}$ values was 58%.

[c] Inhibition of recombinant human NEP activity in a fluorescence assay using 0.15 nM NEP, 2 μM FAM-Gly-Pro-Leu-Gly-Leu-Phe-Ala-Arg-Lys(TAMRA)-NH_2 as substrate in 1 μM $Zn(OAc)_2$, 100 μM TCEP, 50 mM Hepes, 300 μM CHAPS, and 300 mM NaCl at pH = 7.5. The average percent coefficient of variance for the $K_{i\ App}$ values was 43%.

[d] Inhibition of recombinant human CpA activity in a fluorescence assay using 37 nM CpA, 30 μM Abz-Gly-Gly-Nph-OH as substrate in 1 μM $Zn(OAc)_2$, 100 μM TCEP, 50 mM Hepes, 300 μM CHAPS, and 300 mM NaCl at pH = 7.5. The average percent coefficient of variance for the $K_{i\ App}$ values was 38%.

and *neo*-pentyl **1p** (CH_2t-Bu, $K_{i\ App}$ = 7.1 nM) analogs maintained their ACE2 inhibition. Only the bulkier branched analogs, like the α-branched cyclohexyl **1m** (Cyh, $K_{i\ App}$ = 65 nM) and phenyl **1n** (Ph, $K_{i\ App}$ = 84 nM), the β-branched methylene cyclohexyl **1q** (CH_2Cyh, $K_{i\ App}$ = 420 nM) and methylene β-naphthyl **1r** ($CH_2\beta$-Np, $K_{i\ App}$ = 550 nM), and the γ-branched ethylene phenyl **1s** ($(CH_2)_2Ph$, $K_{i\ App}$ = 860 nM), were too large to be accommodated by the ACE2 S^1 subsite.

In contrast, α-branching of the P^1 moiety was poorly tolerated by the ACE S^1 subsite, resulting in substantial decreases in ACE inhibitory activity for the α-branched *iso*-propyl **1h** ($K_{i\ App}$ = 200 nM), (R)-*sec*-butyl **1i** ($K_{i\ App}$ = 490 nM), (S)-*sec*-butyl **1j** ($K_{i\ App}$ = 200 nM), cyclobutyl **1k** ($K_{i\ App}$ = 620 nM), cyclopentyl **1l** ($K_{i\ App}$ = 700 nM), cyclohexyl **1m** ($K_{i\ App}$ = 13,000 nM), and phenyl **1n** ($K_{i\ App}$ = >10,000 nM) analogs. The S^1 subsite of NEP is more accepting of α-branching in P^1 substituents than the ACE enzyme, but less liberal than ACE2. The α-branched *iso*-propyl **1h** ($K_{i\ App}$ = 13 nM), (R)-*sec*-butyl **1i** ($K_{i\ App}$ = 27 nM), (S)-*sec*-butyl **1j** ($K_{i\ App}$ = 2.4 nM), cyclobutyl **1k** ($K_{i\ App}$ = 5.4 nM), cyclopentyl **1l** ($K_{i\ App}$ = 38 nM), cyclohexyl **1m** ($K_{i\ App}$ =1300 nM), and phenyl **1n** ($K_{i\ App}$ = 410 nM) analogs lost some inhibitory activity versus NEP relative to the ethyl analog **1f** ($K_{i\ App}$ = 0.80 nM). Thus, α-branching at the P^1 group enhanced selectivity for ACE2 protease inhibition relative to ACE and NEP. The (R)-*sec*-butyl analog **1i** ($K_{i\ App}$ = 1.5 nM) has 330-fold selectivity versus ACE and 18-fold selectivity versus NEP, while the cyclopentyl **1l** ($K_{i\ App}$ = 1.8 nM) has 390-fold selectivity versus ACE and 21-fold selectivity versus NEP.

In comparison to α-branching, both ACE and NEP S^1 subsites were more permissive to β-branching in P^1 groups. Thus, the *iso*-butyl **1o** analog is not only a potent ACE2 inhibitor ($K_{i\ App}$ = 1.4 nM), but also a low nanomolar ACE ($K_{i\ App}$ = 3.2 nM) and subnanomolar NEP inhibitor ($K_{i\ App}$ = 0.28 nM). ACE is less tolerant of bulky β-branching, with the *neo*-pentyl **1p** analog exhibiting potent dual ACE2 ($K_{i\ App}$ = 7.1 nM) and NEP ($K_{i\ App}$ = 2.6 nM) inhibition with good selectivity over ACE ($K_{i\ App}$ = 2700 nM). Larger β-branched substituents like the methylene cyclohexyl **1q** (ACE2 $K_{i\ App}$ = 420 nM, ACE $K_{i\ App}$ = 840 nM, NEP

$K_{i\ App}$ = 130 nM) and methylene β-naphthyl **1r** (ACE2 $K_{i\ App}$ = 550 nM, ACE $K_{i\ App}$ = 210 nM, NEP $K_{i\ App}$ = 140 nM) attenuate inhibitory activity at all three enzymes. Finally, as the ethylene phenyl analog **1 s** shows, like ACE2 ($K_{i\ App}$ = 860 nM), ACE ($K_{i\ App}$ = 93 nM) was less tolerant of γ-branching in P^1 groups, while NEP ($K_{i\ App}$ = 2.6 nM) accepted it. None of these thiol-based inhibitors was a potent inhibitor of CpA.

A model of the thiol **1i**[19,20] docked into the active site of ACE2 based on the recent X-ray crystal structure[21] is shown in Figure 1. It provides insight into the SAR of the thiol series. In addition to binding to the imidazole nitrogens of ^{374}His and ^{378}His and the carboxylate of ^{402}Glu, the active site zinc coordinates the thiol of the inhibitor. Also, the terminal carboxylate of the inhibitor forms electrostatic interactions with the guanidine of ^{273}Arg and accepts hydrogen bonds from the imidazoles of ^{345}His and ^{505}His. Moreover, the carbonyl of ^{346}Pro accepts a hydrogen bond from the amide nitrogen of the inhibitor, while the amide carbonyl is stabilized by a hydrogen bond to ^{515}Tyr. Furthermore, the $P^{1'}$ methylene biphenyl substituent of **1i** forms significant lipophilic interactions with the quite large $S^{1'}$ channel composed of the lengthwise canal between the two subdomains, including residues ^{274}Phe, ^{276}Thr, ^{346}Pro, ^{367}Asp, ^{370}Leu, ^{371}Thr, and ^{374}His. This biphenyl substituent is hypothesized to occupy a different part of this large pocket than the carboxyl inhibitor co-crystallized in 1R4L. The P^1 (R)-*sec*-butyl group of the inhibitor forms van der Waals interactions with the S^1 pocket composed of ^{347}Thr, ^{504}Phe, ^{510}Tyr, and ^{514}Arg. As shown in the close-up of the S^1 subsite depicted in Figure 2, ^{510}Tyr forms part of a pocket which the α-branched methyl of the P^1 (R)-*sec*-butyl group occupies. Larger substituents are disfavored as they would require movement of the phenol side chain of ^{510}Tyr. Thus, this model agrees with the SAR, since the S^1 subsite can tolerate cyclobutyl and cyclopentyl substituents, but is less accepting of a cyclohexyl group.

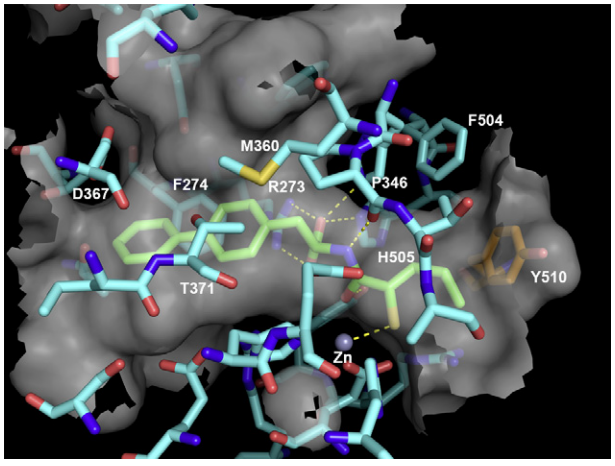

Figure 1. A model of the thiol compound **1i** bound to the active site of ACE2 based on a X-ray co-crystal structure of a carboxylate inhibitor bound to ACE2 (PDB code 1R4L). The ACE2 carbons are colored cyan with inhibitor **1i** carbons colored green. The semi-transparent gray surface represents the molecular surface, while hydrogen bonds are depicted as yellow dashed lines. Several residues were removed for visual clarity. This figure was generated using PYMOL version 1.0 (Delano Scientific, www.pymol.org).

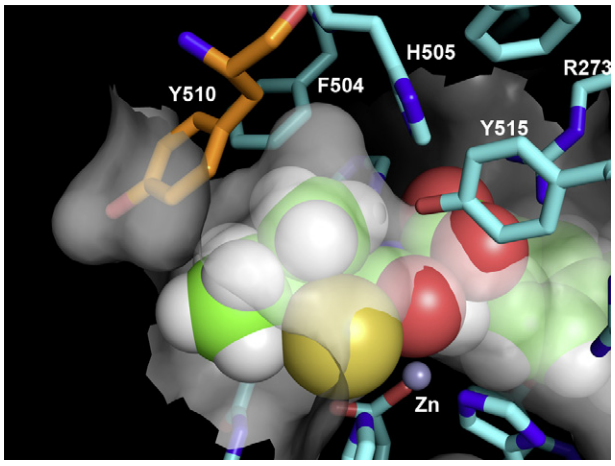

Figure 2. A close up of the P^1 pocket of the model of the thiol compound **1i** bound to the active site of ACE2 based on a X-ray co-crystal structure (PDB code 1R4L). The ACE2 carbons are colored cyan with inhibitor **1i** carbons colored green. ^{510}Tyr is colored in orange to highlight its putative role in the selectivity of **1i**. The semi-transparent gray surface represents the molecular surface. This figure was generated using PYMOL version 1.00 (Delano Scientific, www.pymol.org).

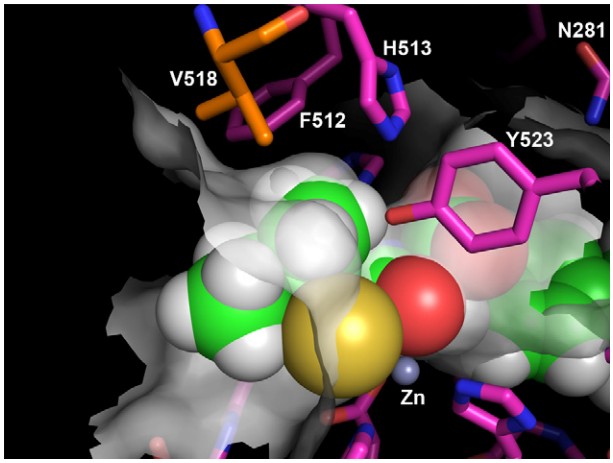

Figure 3. A model of the thiol compound **1i** bound to the active site of ACE using the X-ray co-crystal structure of ACE and lisinopril (PDB code 1O86). The ACE carbons are colored magenta with inhibitor **1i** carbons colored green. ^{518}Val is colored orange to highlight its hypothesized role in the selectivity of **1i**. The semi-transparent gray surface represents the molecular surface. This figure was generated using PYMOL version 1.00 (Delano Scientific, www.pymol.org).

A model of the inhibitor **1i**[19,20] docked into the active site of ACE, focusing on the S^1 subsite, based on the X-ray structure of lisinopril with ACE,[22] is shown in Figure 3. From the model, it is apparent that the methyl group of the (R)-*sec*-butyl P^1 moiety of inhibitor **1i** bumps into the enzyme, helping explain the 330-fold selectivity for ACE2 versus ACE. The branching nature

of ^{518}Val (atom CG1) makes this portion of the S^1 pocket smaller than in ACE2. ^{518}Val is the homologous residue in ACE to ^{510}Tyr in ACE2. This ^{510}Tyr to ^{518}Val substitution from ACE2 to ACE and resulting alteration of the S^1 pocket volume helps explain the reduced ability of ACE to accommodate α-branching in P^1 substituents.

Although X-ray structures of NEP co-crystallized with a thiol-based inhibitor (PDB code 1Y8J)[23] and an analog with a $P^{1'}$ bi-phenyl moiety (PDB code 1R1H)[24] are available, as NEP belongs to a different metalloprotease family (M13 vs M2), no reasonable model of these thiol inhibitors bound to NEP could be determined to help explain the increase in NEP selectivity of α-branched P^1 analogs. Likely protein movement to accommodate potent NEP inhibitors like **1o** is required. The movement of multiple amino acid residues in proteins is difficult to predict accurately.

In summary, a series of α-thiol amide-based inhibitors of ACE2 with varied substituents at the P^1 position were synthesized. Inhibitors containing linear alkyl P^1 moieties were some of the more potent analogs in the ACE2 enzymatic assay. The smaller α-branched P^1 substituents, exemplified by inhibitors **1i** and **1l**, maintained similar potencies, and increased selectivity versus ACE and NEP. Information gained from these studies has proven to be useful in the design of other ACE2 inhibitors. These inhibitors will be reported in due course. Furthermore, a potent pan ACE/ACE2/NEP inhibitor **1o** and a potent dual ACE2/NEP inhibitor **1p** have been identified. These tools may prove useful in further defining the roles these proteases play in the RAS cascade.

Acknowledgment

The authors would like to thank Rob I. West for helpful discussions.

Supplementary data

Supplementary data associated with this article can be found, in the online version, at doi:10.1016/j.bmcl.2007.11.048.

References and notes

1. Donoghue, M.; Hsieh, F.; Baronas, E.; Godbout, K.; Gosselin, M.; Stagliano, N.; Donovan, M.; Woolf, B.; Robison, K.; Jeyaseelan, R.; Breitbart, R. E.; Acton, S. *Circ. Res.* **2000**, *87*, e1.
2. Tipnis, S. R.; Hooper, N. M.; Hyde, R.; Karran, E.; Christie, G.; Turner, A. J. *J. Biol. Chem.* **2000**, *275*, 33238.
3. Danilczyk, U.; Penninger, J. M. *Circ. Res.* **2006**, *98*, 463.
4. Kuba, K.; Imai, Y.; Penninger, J. M. *Curr. Opin. Pharm.* **2006**, *6*, 271.
5. Tallant, E. A.; Ferrario, C. M.; Gallagher, P. E. *Future Cardiol.* **2006**, *2*, 335.
6. Crackower, M. A.; Sarao, R.; Oudit, G. Y.; Yagil, C.; Kozieradzki, I.; Scanga, S. E.; Oliveira-dos-Santos, A. J.; da Costa, J.; Zhang, L.; Pei, Y.; Scholey, J.; Ferrario, C. M.; Manoukian, A. S.; Chappell, M. C.; Backx, P. H.; Yagil, Y.; Penninger, J. M. *Nature* **2002**, *417*, 822.
7. Gurley, S. B.; Allred, A.; Le, T. H.; Griffiths, R.; Mao, L.; Philip, N.; Haystead, T. A.; Donoghue, M.; Breitbart, R. E.; Acton, S. L.; Rockman, H. A.; Coffman, T. M. *J. Clin. Invest.* **2006**, *116*, 2218.
8. Yamamoto, K.; Ohishi, M.; Katsuya, T.; Ito, N.; Ikushima, M.; Kaibe, M.; Tatara, Y.; Shiota, A.; Sugano, S.; Takeda, S.; Rakugi, H.; Ogihara, T. *Hypertension* **2006**, *47*, 718.
9. Donoghue, M.; Wakimoto, H.; Maguire, C. T.; Acton, S.; Hales, P.; Stagliano, N.; Fairchild-Huntress, V.; Xu, J.; Lorenz, J. N.; Kadambi, V.; Berul, C. I.; Breitbart, R. E. *J. Mol. Cell. Cardiol.* **2003**, *35*, 1043.
10. Oudit, G. Y.; Herzenberg, A. M.; Kassiri, Z.; Wong, D.; Reich, H.; Khokha, R.; Crackower, M. A.; Backx, P. H.; Penninger, J. M.; Scholey, J. W. *Am. J. Path.* **2006**, *168*, 1808.
11. Acton, S. L.; Ocain, T. D.; Gould, A. E.; Dales, N. A.; Guan, B.; Brown, J. A.; Patane, M.; Kadambi, V. J.; Solomon, M.; Stricker-Krongrad, A.; PCT Int. Appl. WO 039997, **2002**; *Chem. Abstr.* **2002,** *136*, 402027.
12. Li, W.; Moore, M. J.; Vasilieva, N.; Sui, J.; Wong, S. K.; Berne, M. A.; Somasundaran, M.; Sullivan, J. L.; Luzuriaga, K.; Greenough, T. C.; Choe, H.; Farzan, M. *Nature* **2003**, *426*, 450.
13. Kuba, K.; Imai, Y.; Rao, S.; Gao, H.; Guo, F.; Guan, B.; Huan, Y.; Yang, P.; Zhang, Y.; Deng, W.; Bao, L.; Zhang, B.; Liu, G.; Wang, Z.; Chappell, M.; Liu, Y.; Zheng, D.; Leibbrandt, A.; Wada, T.; Slutsky, A. S.; Liu, D.; Qin, C.; Jiang, C.; Penninger, J. M. *Nat. Med.* **2005**, *11*, 875.
14. Imai, Y.; Kuba, K.; Rao, S.; Huan, Y.; Guo, F.; Guan, B.; Yang, P.; Sarao, R.; Wada, T.; Leong-Poi, H.; Crackower, M. A.; Fukamizu, A.; Hui, C.-C.; Hein, L.; Uhlig, S.; Slutsky, A. S.; Jiang, C.; Penninger, J. M. *Nature* **2005**, *436*, 112.
15. Deaton, D. N.; Gao, E. N.; Graham, K. P.; Gross, J. W.; Miller, A. B.; Strelow, J. M. In *5th General Meeting of the International Proteolysis Society*; Sotiropoulou, G., Pampalakis, G., Arampatzidou, M., Eds.; International Proteolysis Society: Patras, Greece, 2007; p 444.
16. Bhagwat, S. S.; Fink, C. A.; Gude, C.; Chan, K.; Qiao, Y.; Sakane, Y.; Berry, C.; Ghai, R. D. *Bioorg. Med. Chem. Lett.* **1995**, *5*, 735.
17. Hydrolyses were performed under an argon atmosphere. When hydrolyses were carried out with reactions open to the atmosphere, varying amounts of disulfide products were isolated, likely from aerobic oxidation. The enzyme assays contain a reducing agent, tris-(2-chloroethyl)-phosphate (TCEP), to prevent oxidation of the thiols to disulfides during the assays. Dilutions of 10 mM stock solutions of the thiols **1a**–**1s** to final assay concentrations were done with 50% aqueous acetonitrile just prior to protease inhibition studies. Under these standard conditions, both the thiols and their corresponding disulfides showed enzyme inhibitory activity. Presumably, the disulfides were reduced to their corresponding thiols by TCEP during the pre-incubation period, before substrates were added. In contrast, if the assays were performed without TCEP, the disulfides were completely inactive, while the potencies of the thiols were attenuated, probably because of partial aerobic oxidation to their corresponding disulfides during the pre-incubation period.
18. Alcohols **2m** and **2n** are commercially available. Alcohol **2k** was prepared from cyclobutane methanol in three steps. First, oxidation of the alcohol with pyridinium chlorochromate afforded the aldehyde. Then, reaction of the aldehyde with trimethylsilyl cyanide and *N*-methyl morpholine N-oxide provided the silyl protected cyano-

hydrin. Finally, hydrochloric acid catalyzed hydrolysis of the cyanohydrin yielded the hydroxyacid **2k**.

19. Lambert, M. H. In *Practical Application of Computer-Aided Drug Design*; Charifson, P. S., Ed.; Marcel Dekker: New York, 1997; p 243.
20. The 'grow' algorithm within the MVP program was used to dock the inhibitor into the active site beginning from the carboxylic acid group.
21. Towler, P.; Staker, B.; Prasad, S. G.; Menon, S.; Tang, J.; Parsons, T.; Ryan, D.; Fisher, M.; Williams, D.; Dales, N. A.; Patane, M. A.; Pantoliano, M. W. *J. Biol. Chem.* **2004**, *279*, 17996.
22. Natesh, R.; Schwager, S. L. U.; Sturrock, E. D.; Acharya, K. R. *Nature* **2003**, *421*, 551.
23. Sahli, S.; Frank, B.; Schweizer, W. B.; Diederich, F.; Blum-Kaelin, D.; Aebi, J. D.; Boehm, H.-J.; Oefner, C.; Dale, G. E. *Helv. Chim. Acta* **2005**, *88*, 731.
24. Oefner, C.; Roques, B. P.; Fournie-Zaluski, M. C.; Dale, G. E. *Acta Crystallogr. D: Biol. Crystallogr.* **2004**, *60*, 392.